

## Detecting and modelling the collapsed zone around a shaft in a dam site by microgravity data

V.E. ARDESTANI<sup>1, 2</sup> and Z.B. ASHENA<sup>1</sup>

<sup>1</sup> *Institute of Geophysics, University of Tehran, Iran*

<sup>2</sup> *Center of Excellency in Survey Engineering and Disaster Management, Tehran, Iran*

(Received: January 23, 2017; accepted: March 6, 2018)

**ABSTRACT** The low-density regions caused by collapsed zones can be delineated and modelled in dam sites by microgravity data. After measuring the data and using standard correction methods, the Bouguer anomalies are computed. The residual anomalies are obtained by removing the trend or regional anomalies from Bouguer anomalies. The negative anomalies, which are caused by low-density zones, can be readily distinguished in a residual anomaly map. Detecting and modelling these zones could prove a difficult task in dam sites due to the likely rough topography and construction activities in and around the sites. A collapsed zone in and around a shaft is detected and modelled in the Siah-Bisheh dam site in the Alborz Mountains in northern Iran.

**Key words:** collapsed zone, dam site, microgravity data, detecting and modelling.

### 1. Introduction

The difference in the densities of subsurface materials is the basic concept of microgravity surveys. Microgravity is an effective tool to detect areas (zones) of contrasting or anomalous density by measuring the variation of the gravity acceleration of the Earth. One of the main sources of local lows in microgravity data are the low-density zones caused by cavities and collapsed zones in mining and dam sites.

These underground collapsed zones caused by man-made cavities including mine workings, shafts and tunnels, are hazardous and can even be more prevalent than natural features, particularly in industrialized environments. The collapsed zones represent a mass deficiency in the subsurface that generate negative anomalies.

Several examples of promising microgravity surveys have been carried out in the past decades over large features including natural and man-made cavities such as: Patterson *et al.* (1995), Cooper (1998), Styles *et al.* (2005, 2006), and Ardestani (2008, 2014). The object of these and many other published papers concern natural cavity detection in the rocks but only a few examples of microgravity surveys deal with the application of the method in detecting man-made cavities or collapsed zones.

## 2. Site character and geology

The site under investigation is located in a mountainous area in the Alborz Mountains, in northern Iran. The location of the site is shown in Fig. 1. The coordinates of the base point which is located at the microgravity grid is 36.228° W longitude and 51.304° N latitude.

The microgravity grid is designed to be above an oblique tunnel that crosses the collapsed zone. The geological map is shown in Fig. 2.

The dominant geological formations are the Nesen, Elika and Dorod (Attarzadeh, 2009). The main units of these formations are Cretaceous limestone and alternative layers of shale mudstone and sandstone of the uppermost Jurassic (Tithonian). Fractured zones, karst cavities, and shear zones are the result of the very active tectonic regime of the survey area.



Fig. 1 - Location of the site.

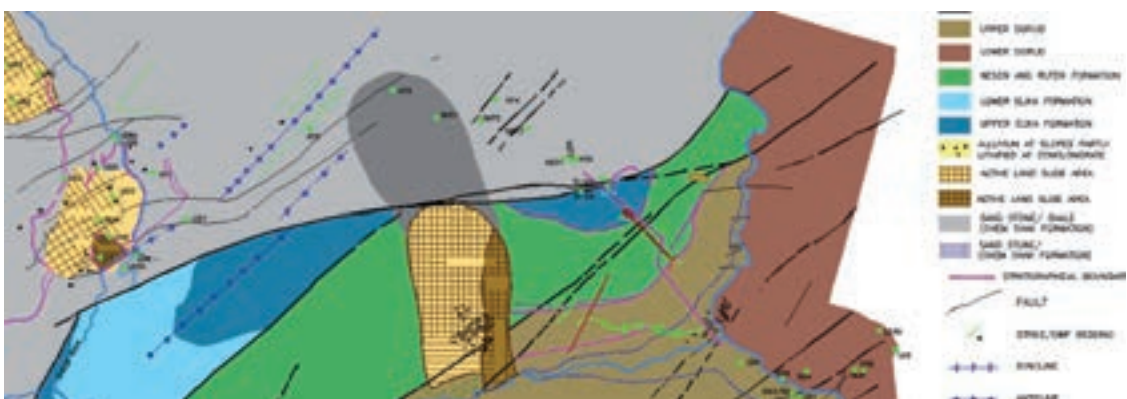


Fig. 2 - Geological map.

Three shafts have been excavated in the area; all of these shafts passed or reached the main thrust fault zone that can be seen in Fig. 2 and are located in the middle of the microgravity survey area. There is a collapsed zone around and in one of these shafts that has obstructed the shaft. To detect and model this zone is the main object of this survey. The microgravity survey area is shown in Fig. 1 with a black box.

### 3. Field procedure of microgravity survey

The microgravity survey was conducted in the area with dimensions of about 200 m by 170 m including 160 measurement points and with a basic grid dimension of 15 m.

The gravity network is designed over the collapsed zone. Data were collected with a CG3-M gravimeter with a sensitivity of approximately 1  $\mu$ Gal. The coordinates of the points have been measured by a RTK dual frequency GPS (Trimble R7, R8) with an accuracy less than 1 cm in positioning and elevation.

### 4. Gravity corrections

A local base point was selected in the area and all the measurements have been referenced to this point and measured several times in a working day for drift correction. The absolute value of gravity has been transferred to the base.

The long-term drift of gravimeter has been removed by continuous reading (cycling mode) at the Institute of Geophysics (University of Tehran). To remove the short-term drift, the measurements were repeated at the base point each hour of the working day and the maximum drift was equal to 10  $\mu$ Gal. The Bouguer density has been obtained from the comprehensive geological surveys and excavated boreholes in the dam site and is equal to 2600 kg/m<sup>3</sup>. To compute Bouguer anomalies, a standard approach has been followed. In order to determine the precision of the measurements, the measurement was repeated on 20% of the stations. Based on the values obtained from the repeated surveys, a MSE of a single measurement has been calculated as 0.009 mGal. This value is not too far from the standard field repeatability of the CG-3M (0.005 mGal) and considering the rough topography of surrounding area, it is fairly satisfactory. The following relation has been applied for the computation of the Bouguer anomaly:

$$\Delta g = g_{obs} + (\delta gf - \delta gB + \delta gt) - \gamma_0 \quad (1)$$

where  $g_{obs}$  is measured gravity,  $\delta gf$  is free-air correction,  $\delta gB$  is Bouguer correction,  $\delta gt$  is terrain corrections, and  $\gamma_0$  is the normal gravity value.

The terrain correction is usually the most sensitive stage in gravity reductions. This correction was calculated using a combination of the methods described by Kane (1962) and Nagy (1966). To calculate the local corrections, the local digital terrain model (DTM) was "sampled" to a grid mesh centred on the station to be calculated. The grid sampled spacing in the local and regional grids were 5 and 10 m, respectively. The correction was calculated based on near zone and far zone contributions and applying the local and regional grids. In the near zone (0 to 1 cells from the station), the algorithm sums the effects of four sloping triangular sections, which describe a

surface between the gravity station and the elevation at each diagonal corner by the following equation (Kane, 1962):

$$g_i = G\rho\Phi \left( R - \sqrt{R^2 + H^2} + \frac{H^2}{\sqrt{R^2 + H^2}} \right) \tag{2}$$

where  $g_i$  is the gravity effect,  $G$  is the gravitational constant,  $\rho$  is the density,  $R$  is the length of the triangle,  $H$  is the elevation at the diagonal corner, and  $\Phi$  is the horizontal angle between the station and the horizontal diagonal corners.

In the far zone (1 to end cells from the station), the terrain effect was calculated for each point using the flat-topped square prism approach of Nagy (1966):

$$g = -G\rho \left[ \begin{matrix} z2 \\ z1 \end{matrix} \left| \begin{matrix} y2 \\ y1 \end{matrix} \right| \begin{matrix} x2 \\ x1 \end{matrix} \right] x \cdot \ln(y + R) + y \cdot \ln(x + R) + zt g^{-1} \left( \frac{z \cdot R}{x \cdot y} \right) \tag{3}$$

where  $g$  is the gravity effect of the prism,  $G$  is the gravitational constant,  $\rho$  the density and  $x1, y1, z1$  and  $x2, y2, z2$  are the Cartesian coordinates of the left lowermost and right uppermost corners of the prism in a right angle coordinate system, respectively and

$$R = \sqrt{x^2 + y^2 + z^2} \tag{4}$$

As the height of the gravity points were measured accurately, we included these points in the DTM to make it as dense as possible. The adjacent topography of the gravity network up to 1000 m was also surveyed. Terrain corrections using the presented formulas and microgravity network are presented in Fig. 3.

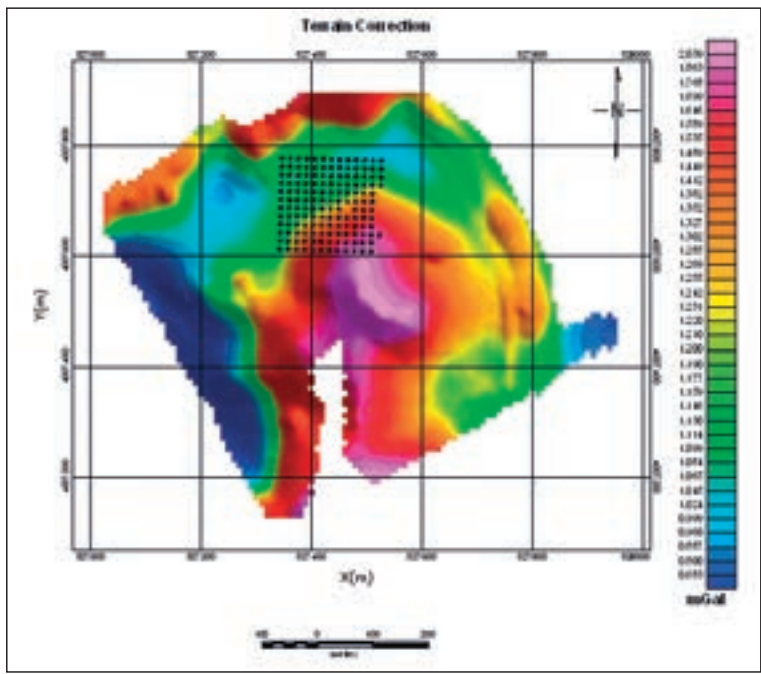


Fig. 3 - Terrain correction.

The statistical values for topographical corrections and Bouguer anomalies in the measured points are reported in Table 1.

Table 1 - Statistical values for terrain correction and Bouguer anomalies.

Values	Minimum (mGal)	Maximum (mGal)	Average (mGal)	Standard Deviation (mGal)
Terrain Corrections	0.54	2.47	1.27	0.31
Bouguer Anomalies	-88.02	-85.09	-86.38	0.406

As can be seen in this table, the standard deviation of terrain correction is less than the Bouguer anomalies. Therefore, by considering the rough topography of the survey area and the limited coverage of digital terrain model, the values in Table 1 show an acceptable accuracy for terrain corrections.

### 5. Data processing

After the prescribed corrections, the Bouguer gravity anomalies are computed through Eq. 1 and shown in Fig. 4. We have subtracted regional anomalies, constructed by a two degrees polynomial, from the Bouguer anomalies to calculate the residual anomalies and the results are given in Fig. 5.

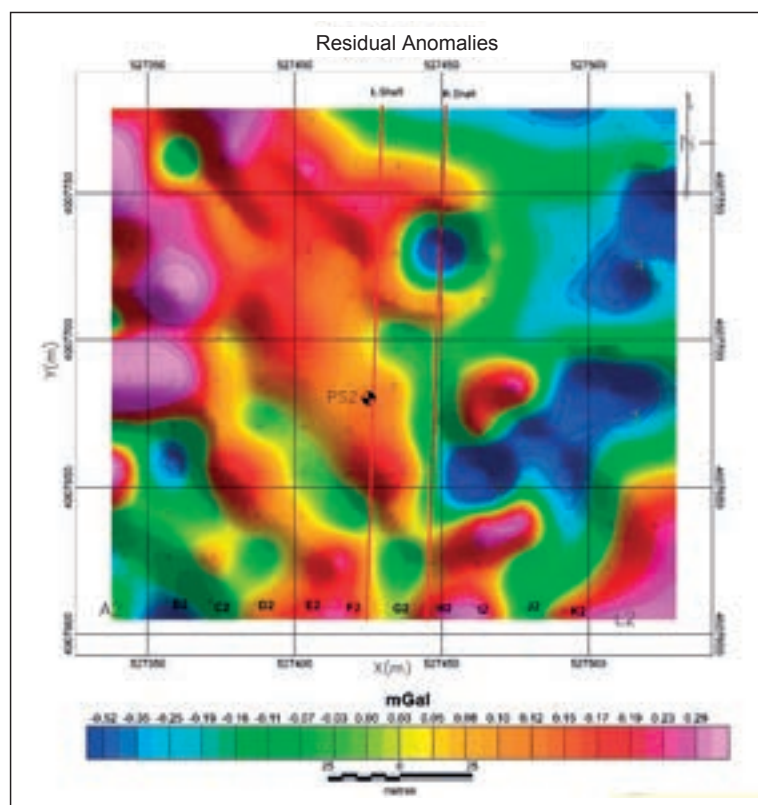


Fig. 4 - Bouguer anomalies.

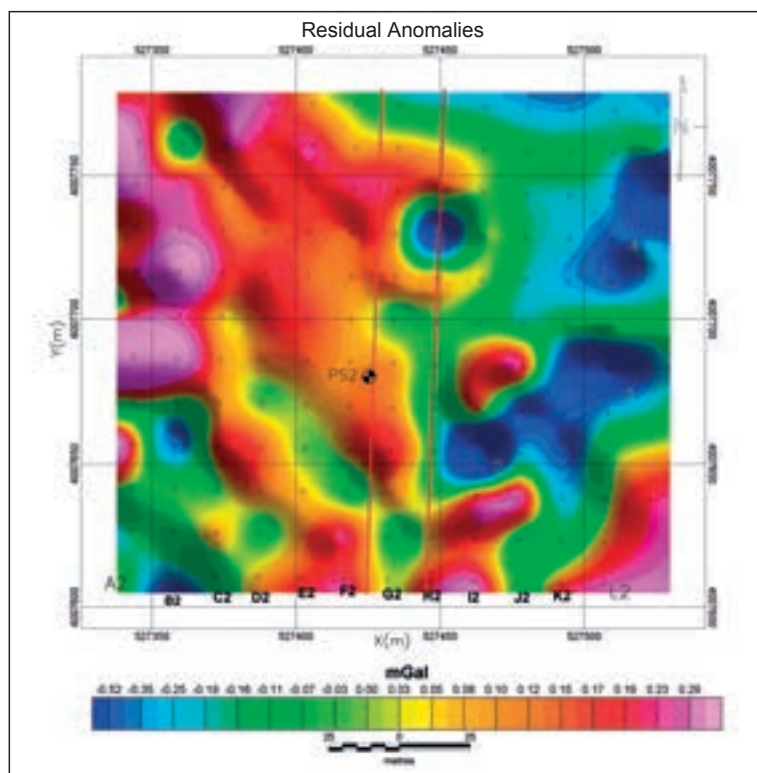


Fig. 5 - Residual anomalies.

Observing the Bouguer gravity anomalies in Fig. 4, several relative negative anomalies caused by low-density zones are distinguished and numbered from 1 to 4.

The negative anomalies are also numbered from 1 to 4 in Fig. 5. The projection of the walls of the pressure shaft and the borehole close to it (PS2) are also shown in Figs. 4 and 5.

In order to estimate the maximum depth of these anomalies, the principle by Jacobson (1987) has been used and the results are reported in Figs. 6 and 7. In this principle, the distance of upward continuation is considered as the depth of the downward continuation. The distance at which the effects of the anomalies disappear will be considered as the maximum depth. The upward continuation has been computed using the Oasis Montaj (Version 7) software. Considering Figs. 6 and 7, the maximum depth of the number 1 and 2 anomalies is less than 10 m and is not clear and erroneous for the number 3 and anomalies 4 due to their regional trend at the corner of the network.

Although the shape and the location (close to the pressure shaft) of the number 1 and 2 anomalies make them probable candidates for the collapsed zone, their maximum depths is in contrast with this assumption. These detected anomalies are generated by shallow low-density zones caused by fractured zones and small karstic areas.

The target collapsed zone is not represented by existing negative anomalies in Bouguer and residual anomalies maps (Figs. 4 and 5).

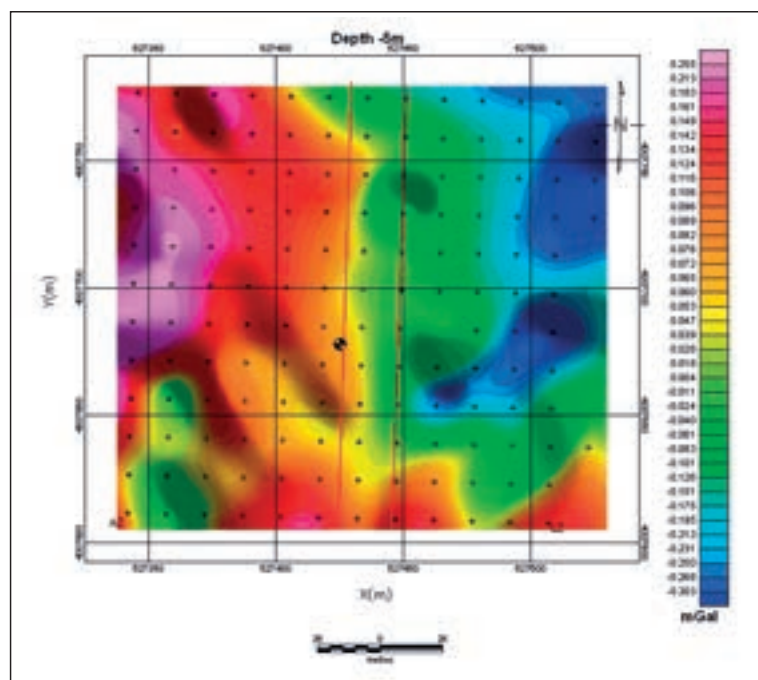


Fig. 6 - Upward continuation (5 m).

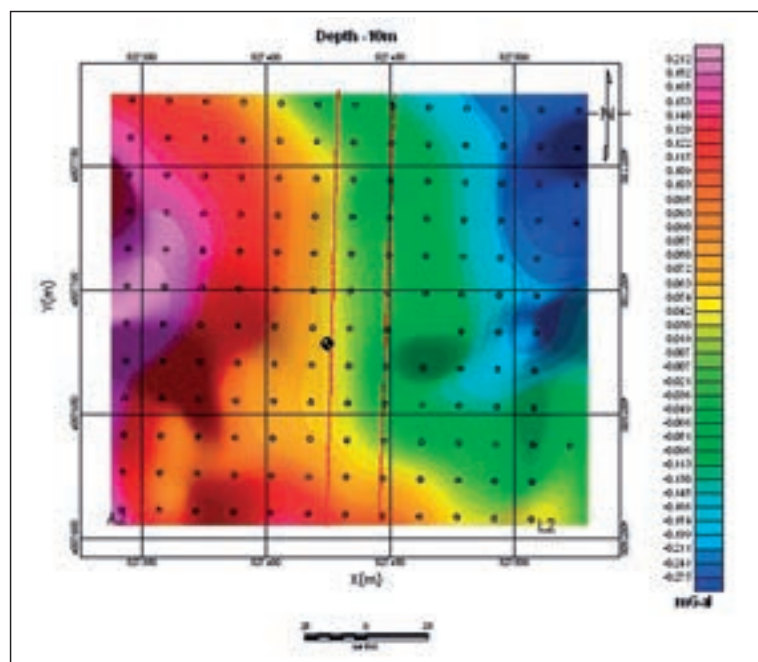


Fig. 7 - Upward continuation (10 m).

### 6. 3D Modelling

To simulate and model the collapsed zone, a 3D inversion algorithm described by Camacho *et al.* (2002) is applied. This method aims to determine the geometry of subsurface gravity anomalies with prescribed (fixed or variable) density contrasts.

Both positive and negative density contrasts can be applied. In this method, the subsurface is

divided into prismatic cells and the algorithm seeks to determine the anomalous bodies by means of a “growth” sequence, analysing the several model possibilities.

This algorithm has been successfully applied by the author in several other projects and the results have been published in pioneer papers such as Ardestani (2008, 2014, 2015).

The results of the 3D modelling are presented in Figs. 8 to 16. Figs. 9 to 16 show cross-sections along the N-S profiles that are shown in Fig. 4 and named from A to L, eastwards. It is worth mentioning that the algorithm considers the horizontal ground surface and so in the case of rough topography the results are not reliable above the terrain surface. Therefore, for the sake of clarity, the ground surface is shown in Figs. 9 to 16.

In Figs. 10 to 15, the collapsed zone can be distinguished from profile B to H and in the N-S direction dipping toward south very clearly.

The most important result from these figures is the modelling of the collapsed zone: it begins from 2290 m height and extends to 2200 m with a length of at least 90 m.

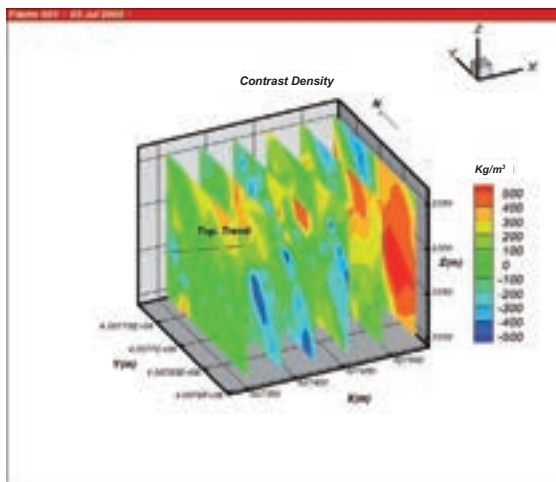


Fig. 8 - 3D contrast density.

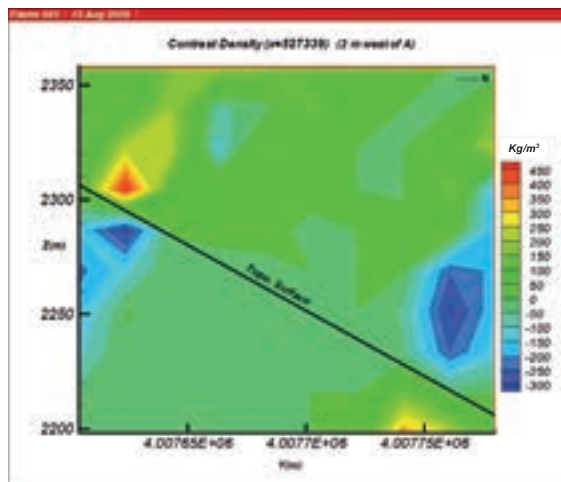


Fig. 9 - Cross section of contrast density along  $x=527339$ .

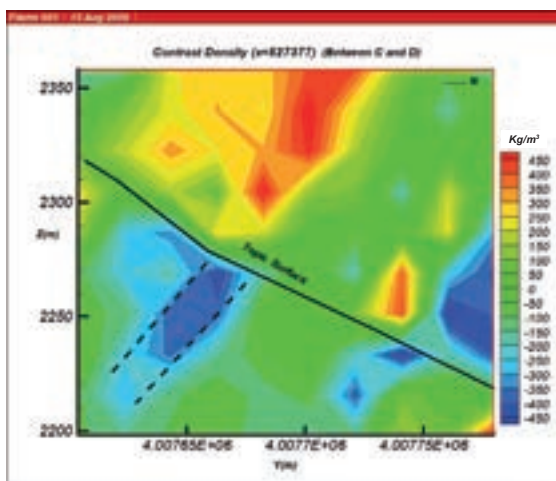


Fig. 10 - Cross section of contrast density along  $x=527377$ .

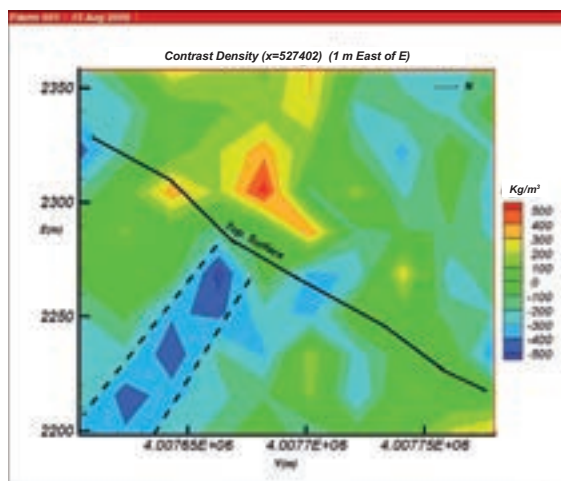


Fig. 11 - Cross section of contrast density along  $x=527402$ .

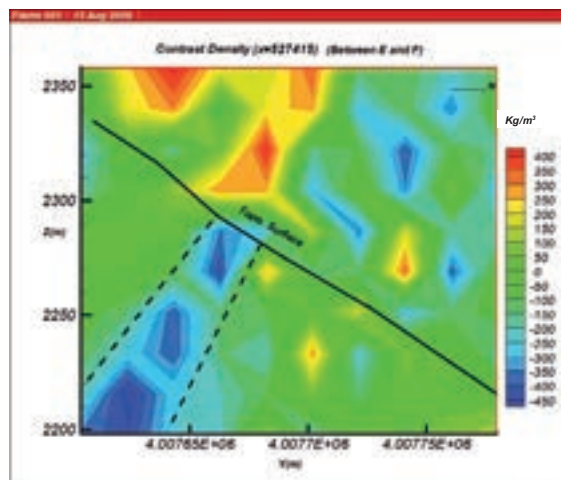


Fig. 12 - Cross section of contrast density along x=527415.

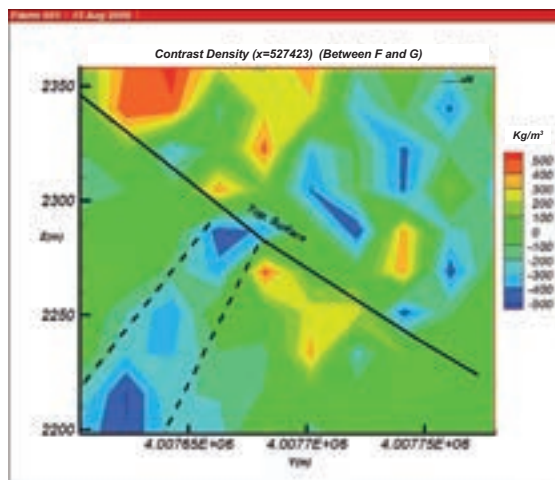


Fig. 13 - Cross section of contrast density along x=527423.

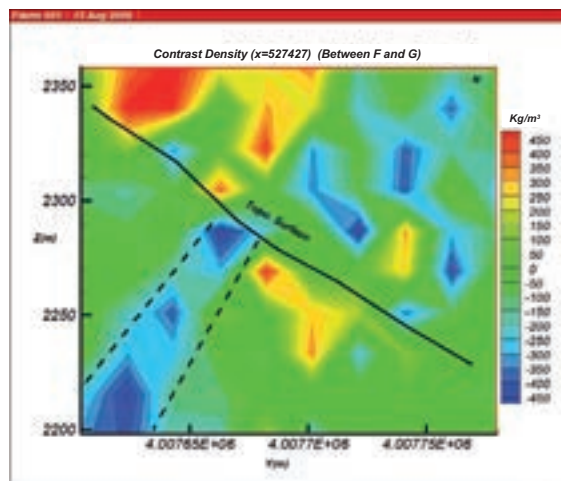


Fig. 14 - Cross section of contrast density along x=527427.

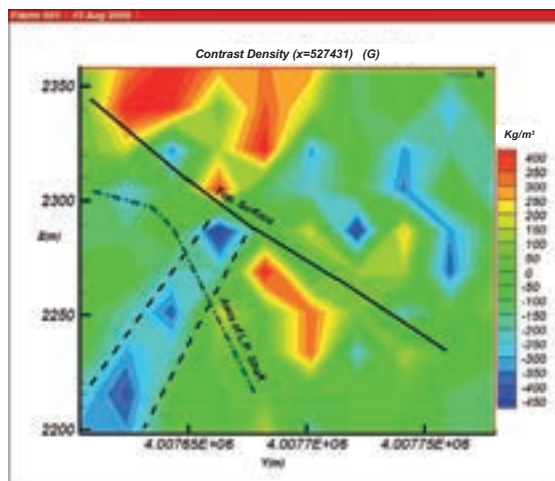


Fig. 15 - Cross section of contrast density along x=527431.

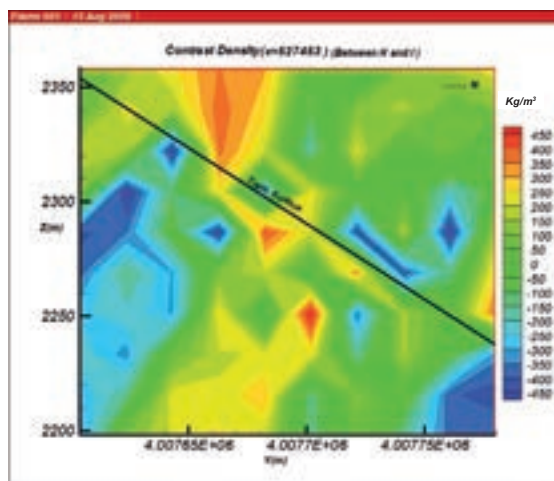


Fig. 16 - Cross section of contrast density along x=527453.

## 8. Conclusions

Microgravity surveys are a valuable method to detect voids and low-density subsurface anomalies in general. The method can be applied in dam sites and abandoned mines to detect collapsed zones, buried galleries or inaccessible shafts. On the other hand, some of these anomalies, which are not reflected in Bouguer or residual anomaly maps, can be modelled by existing efficient algorithms. In this current survey, a collapsed zone is modelled precisely even in this rough topography and in the location that does not show visible surface gravity anomalies in Bouguer or residual maps. The geometrical and physical characteristics of the main anomaly is modelled and it coincides with the strike and dip of the proposed shaft.

**Acknowledgments.** The author is very thankful to the authorities of the Institute of Geophysics, University of Tehran for all their support. Special thanks are due to Eng. Salimi for measuring the field data.

## REFERENCES

- Ardestani V.E.; 2008: *Modelling the Karst zones in a dam site through micro-gravity data*. Explor. Geophys., **39**, 204-209.
- Ardestani V.E.; 2014: *Detecting and modelling the evaporate dome in a dam site using microgravity data*. Boll. Geof. Teor. Appl., **55**, 683-697.
- Ardestani V.E.; 2015: *Detecting, modeling and reserve estimating of manganese ore bodies via microgravity data*. Boll. Geof. Teor. Appl., **56**, 19-30.
- Attarzadeh A.; 2009: *Geological map of the project area*. Moshanir Power Consulting Eng.
- Camacho A.G., Montesinos F.G. and Viera R.; 2002: *A 3-D gravity inversion tool based on exploration of model possibilities*. Comput. Geosci., **28**, 191-204.
- Cooper A.H.; 1998: *Subsidence hazards caused by the dissolution of Permian gypsum in England: geology, investigation and remediation*. Geohazards Eng. Geol., Eng. Special Publ., **15**, 265-275.
- Jacobson H.; 1987: *A case for upward continuation as a standard separation filter for potential field maps*. Geophys., **52**, 1138-1145.
- Kane M.F.; 1962: *A comprehensive system of terrain corrections using a digital computer*. Geophys., **27**, 455-467.
- Nagy D.; 1966: *The gravitational attraction of a right rectangular prism*. Geophys., **31**, 362-371.
- Patterson D.A., Davey J.C., Cooper A.H. and Ferris J.K.; 1995: *The investigation of dissolution subsidence incorporating microgravity geophysics at Ripon*. Q. J. Eng. Geol. Hydrogeol., **28**, 83-94.
- Styles P., McGrath R., Thomas E. and Cassidy N.J.; 2005: *The use of microgravity for cavity characterization in karstic terrains*. Q. J. Eng. Geol. Hydrogeol., **38**, 155-169.
- Styles P., Toon S., Thomas E. and Skittiral M.; 2006: *Microgravity as a tool for the detection, characterization and prediction of geohazard posed by abandoned maining cavities*. First Break, **24**, 51-60.

**Corresponding author:** Vahid E. Ardestani  
 Institute of Geophysics, University of Tehran and Center of Excellency in Survey Engineering and Disaster Management, Teheran, Iran  
 Phone: +98-21-61118232; Fax: +98-21-88630548; e-mail: ebrahimz@ut.ac.ir